

Feasibility of Multiparametric Imaging with PET/MR in Head and Neck Squamous Cell Carcinoma

Running head: Multiparametric imaging in HNSCC

Jacob H. Rasmussen^{1,2}, Martin Nørgaard^{3,4}, Adam E. Hansen³, Ivan R. Vogelius¹, Marianne C. Aznar¹, Helle H. Johannesen³, Junia Costa³, Astrid ME. Engberg³, Andreas Kjær³, Lena Specht¹, Barbara M. Fischer³

¹Department of Oncology, Section of Radiotherapy, Rigshospitalet, University of Copenhagen, Denmark.

² Department of Otorhinolaryngology, Head & Neck Surgery and Audiology, Rigshospitalet, University of Copenhagen, Denmark.

³Department of Clinical Physiology, Nuclear Medicine and PET, Rigshospitalet, University of Copenhagen, Denmark.

⁴Neurobiology Research Unit, Rigshospitalet, University of Copenhagen, Denmark.

Conflicts of interest: None

Corresponding author:

Jacob H Rasmussen, MD, PhD

Department of Otorhinolaryngology, Head & Neck Surgery and Audiology

Rigshospitalet F-2074

Blegdamsvej 9

2100 Copenhagen

Denmark

Word count: 4752 (incl. References)

ABSTRACT:

Purpose. The purpose of this study was to investigate and assess the correlation and the reproducibility of multiparametric imaging in head and neck cancer patients.

Material and Methods. Twenty-one patients were included in this prospective scan-rescan study. All patients were scanned twice on an integrated Positron Emission Tomography and Magnetic Resonance imaging scanner (PET/MR). Gross tumor volumes (GTV) were defined on T₂-weighted MR images (GTV_{T2}) and volumes of interest were defined on diffusion-weighted magnetic resonance imaging and FDG PET (VOI_{DWI}, VOI_{PET}). Overlap between volumes was assessed as a percent-wise overlap. FDG uptake and diffusion were measured using standardized uptake value (SUV) and apparent diffusion coefficient(ADC) and correlation was tested across and within patients and as a voxel-by-voxel analysis.

Results. Seventeen patients were available for correlation analysis and 12 patients were available for assessment of tumor overlap. The median tumor overlap between VOI_{DWI} and VOI_{PET} was 82%(VOI_{DWI} in VOI_{PET}) and 62%(VOI_{PET} in VOI_{DWI}) on scan 1 and scan 2, respectively. Across patients, the correlation between SUV and ADC was weak and non-significant. However, in individual patients a weak but significant correlation was identified on a voxel-by-voxel basis.

Conclusion. In multiparametric imaging with the integrated PET/MR, the VOIs from DWI and FDG PET were both within the target volume for radiotherapy and overlapped substantially although not completely. No correlation between FDG uptake and DWI could be found across patients, but within individual patients a statistically significant, but weak, voxel-by-voxel correlation was found. The findings suggest that information on glucose uptake and diffusion coefficient carries complementary information of interest which may be relevant for radiotherapy treatment planning.

INTRODUCTION

The concept of personalized medicine has brought increased awareness to inter- and intra-tumor heterogeneity (1) and the evidence supporting the importance of considering tumor heterogeneity in therapy planning is increasing (2–4). Single tumor biopsies cannot account for intra-tumor heterogeneity and it is not realistic to perform multiple biopsies of individual tumors or to biopsy all

lesions in individual patients with metastatic disease in an attempt to assess intra- or inter-tumor heterogeneity. Therefore a new diagnostic method, which can provide a more comprehensive view of the tumor biology, including intra-tumor heterogeneity is warranted. Tumor heterogeneity can now be investigated with multiparametric imaging(5,6) and in this respect, hybrid-imaging with PET/MR (integrated Positron Emission Tomography and Magnetic Resonance imaging) provides a promising and non-invasive alternative(7–9).

Squamous cell carcinoma of the head and neck (HNSCC) is a heterogeneous disease (10–12) and with the introduction of PET/MR imaging it is now possible to assess some of this heterogeneity by comparing two functional imaging techniques simultaneously on a voxel-by-voxel basis. For example comparisons can be made between diffusion weighted imaging (DWI) and 18F-fluorodeoxyglucose, (FDG) both of which can be quantified, DWI as apparent diffusion coefficient (ADC) and FDG uptake as the standardized uptake value (SUV).

Low ADC and high SUV have both been reported to correlate with poor patient outcome (13,14). DWI and FDG PET can potentially offer complementary information in HNSCC (15,16) and it is hypothesized that biologically different sub-volumes can be identified with functional imaging and targeted with radiation dose painting (17). Integrated PET/MR can provide DWI and FDG uptake simultaneously reducing misalignment due to time, positioning, and biologic changes, thus allowing assessment of several relevant dose painting targets and the concordance between such targets. Several studies have stated that ADC and SUV may be important parameters in describing heterogeneity and defining sub-volumes within GTV for dose painting. Both PET and DWI may reflect various functional properties of tumor tissue, although this approach obviously requires that the sub-volumes are stable over time and lie within the actual target volume. The correlation between ADC and SUV has been explored by several research groups and for various tumor types. In general, there is a consensus that a negative correlation between the minimum ADC-value and the maximum SUV-value exists (18–20). Schmidt et al. 2013(21) suggested that a voxelwise correlation of ADC and FDG PET using PET/MR might provide a more sophisticated spatial characterization of tumors, as did Metz et al. in 2015 (22). To the best of our knowledge this is the first study evaluating the correlation between DWI and FDG PET on a voxel-wise basis as well as scan-rescan stability on an integrated PET/MR scanner in patients with HNSCC.

The hypothesis of this study is that there is a strong and reproducible correlation between FDG PET and DWI both by ADC/SUV measures and by volume of interest. Here, 'strong' should be interpreted as sufficiently reliable correlation to allow assessment of ADC from the SUV uptake in a voxel and vice-versa with sufficient accuracy for clinical use. The following four specific aims are addressed in order to test the hypothesis of the study.

(1) Investigate and quantify the overlap between the tumor volumes defined by DWI and FDG PET images simultaneously on an integrated PET/MR scanner and report the reproducibility.

(2) Investigate the correlation between FDG uptake (SUV) and apparent diffusion coefficient (ADC) across patients.

(3) Investigate the voxel-wise correlation of FDG uptake and ADC.

(4) Explore the potential of an unsupervised cluster analysis of joint FDG and ADC data to identify tumor sub-volumes.

MATERIAL AND METHODS

Patients

Twenty one patients were included in this prospective scan-rescan study after written informed consent. The patients were scanned twice with exactly three days apart. All patients in the present study were from a patient cohort of 30 patients originally included in a study designed to test reproducibility of FDG uptake on both PET/CT and PET/MR(23). The study was approved by the local ethics committee, approval number H-3-2012-072.

¹⁸F-FDG PET/MR

All patients were scanned on the same integrated PET/MR system (Siemens Biograph mMR)(24) with a 3 T magnet using a head and neck coil. Patients were instructed to fast for minimum six hours and scanned 100-120 minutes after injection of FDG (4 MBq/kg). The time interval between FDG

injection and time to scan on the second scanning day was attempted to match the actual time interval on the first scanning day.

PET was performed as a single-bed, 20 min acquisition. PET data were reconstructed using OP-OSEM with 3 iterations, 24 subsets and 4 mm Gaussian post filter into 344 x 344 matrices. Resolution modeling (PSF) was not applied.

A T₂-weighted sequence was acquired, followed by a Dixon VIBE sequence for attenuation correction purposes. All scans were performed without a gadolinium contrast agent. The imaging protocol for the DWI consisted of a 2D echoplanar sequence (EPI) with matrix size = 92 x 92 x 24; voxel size = 2.71 x 2.71 x 4 mm; TR/TE = 3000/84 ms; parallel imaging factor (GRAPPA) = 4, flip angle = 90° and was performed in all patients with 3 different b-values (0, 500, 1000 s/mm²). DWI was measured as 3 stacks, each at isocenter to maximize field homogeneity. DWI had an effective echo spacing of 0.145 ms. and DWI distortions were corrected using the an algorithm (FUGUE) of the FSL software package(25) (Analysis Group, FMRIB, Oxford, UK).

Definitions of volume of interest

A region of interest covering the primary T-site was defined on MR and PET, respectively. The PET images were assessed by a specialist in nuclear medicine (BMF) and the FDG PET positive tumor volume i.e. volume of interest (VOI_{PET}) was defined and delineated manually. This was done by a visual adaptation of an SUV iso-contour starting at 40% of the maximum standardized uptake value (SUV_{max}) so as to include the steepest gradient of SUV-avid tissue and exclude physiological FDG uptake(26).

The diffusion weighted imaging was assessed by a MR-radiologist (HHJ). Prior to the delineation of the volume of interest defined from DWI (VOI_{DWI}), the PET and anatomical images were assessed to exclude patients with a large signal drop out or other severe artifacts on DWI. An example of signal drop out can be seen in the supplement material (Supplemental Fig. 1). The radiologist did not have access to the PET imaging during the actual delineation of the VOI_{DWI}, likewise the specialist in nuclear medicine did not have access to the MR scan during the delineation.

The definition and delineation of the anatomical gross tumor volume on MR (GTV_{T2}) was performed by a radiologist specialized in tumor delineation (JC). The delineation was performed on the T_2 -weighted images without access to or prior evaluation of the functional images (i.e. both PET and DWI). The tumor volume was delineated as a target volume for radiotherapy, i.e. if there was doubt regarding tumor extension it was included in the GTV_{T2} . The MR defined target volume (GTV_{T2}) was chosen to ensure that the volumes defined from FDG PET and DWI were within the relevant target volume for radiotherapy.

Analysis of DWI and PET data

SUV, ADC and volume metrics were extracted from the software package Mirada XD3 (MIRADA Medical, Oxford, UK). Tumor volume overlap between the respective imaging modalities was assessed as a percent-wise overlap.

In addition, a voxel-wise analysis of PET, T_2 -weighted MR images (T_2 -MRI) and DWI was executed using MATLAB R2014b (8.4.0.150421) 64bit. PET and T_2 -MRI were initially resampled to the same dimensions as the ADC sequence (92 x 92 x 24 voxels; voxel spacing 2.71 x 2.71 x 4 mm) in OsiriX v.5.7.1 32bit, so the dimensions of the PET, T_2 -MRI and ADC sequences were all in accordance prior to a voxel-wise analysis. PET and DWI volumes-of-interest were imported from Mirada and resampled to the ADC sequence. All voxels present in the delineated volumes-of-interests were used in the voxel-wise analysis. A Gaussian Mixture Model was used as a data-driven cluster analysis to cluster specific voxels according to their likelihood of belonging to a certain sub-volume (e.g. a multivariate normal distribution), as previously described by Schmidt et al.(21). In our specific context it was assumed that a small area in the tumor (voxel), belonged to a certain sub-volume (for example representing underlying biological tissue characteristics, such as inflammation, necrosis, malignant tissue, benign tissue etc.) defined by a multivariate normal distribution with cluster-specific mean and covariance. On visual assessment the tumors did not appear heterogeneous and thus the analysis was restricted to search for two clusters, and the cluster with the highest SUV was called cluster 2.

Statistical Analysis

Statistical analysis was performed in SPSS version 19. The reproducibility of SUV and ADC values were assessed using the paired T-test. Correlations between SUV_{max} and ADC_{min} , and SUV_{mean} and ADC_{mean} , respectively, on both scans were assessed using Pearson's correlation. Correlation of the distribution of ADC and SUV in a voxel-wise comparison was assessed using Spearman's rank correlation.

RESULTS

Patients

Twenty-one patients were scanned twice with PET/MR as previously described (23). Four patients had to be excluded due to a large signal drop out at the tumor site on the DWI caused by geometric distortion (supplemental Fig. 1), leaving 17 patients available for further analysis of correlation between SUV and ADC. After the FUGUE correction no patients had to be excluded due to signal drop out. In four other patients FUGUE correction was not possible in neither of the two scans and in another two patients FUGUE correction was only possible in one of the two scans. Leaving 12 patients available for assessment of tumor overlap between FDG PET and DWI and for the voxel-by-voxel comparison (11 + one with FUGUE correction from the first scan and 11 + the other with FUGUE correction data from the second scan). The reproducibility of tumor overlaps and voxel-wise comparison was therefore feasible in a total of 11 patients who had all data available from both PET/MR scans. A flowchart of patient inclusion can be seen in Fig. 2 and Table 1 summarize the number of patients with data available from the first and the second scan.

Overlap of tumor volumes

The volumes from the three imaging modalities measured on scan 1 and 2 respectively are illustrated in Fig. 1. The median tumor volume and the median tumor overlap between the three different imaging modalities can be seen in Table 2. For all cases $VOI_{DWI} < VOI_{PET} < GTV_{T2}$. As expected the gross tumor volume assessed with both DWI (VOI_{DWI}) and FDG PET (VOI_{PET}) was encompassed in the anatomically defined tumor volume (GTV_{T2}) on both, the first and the second scan, respectively 98% and 99% (Table 2). In all but one case, more than 73% of the tumor volume defined from DWI was encompassed in VOI_{PET} . In the remaining case, only 58% and 48% of VOI_{DWI} was

encompassed in VOI_{PET} on the first and second scan, respectively. The median tumor overlap was above 80% (VOI_{DWI} within VOI_{PET}) on both scan 1 and 2 and proved to be reproducible (Table 2). The difference in overlap from scan 1 to scan 2 was small (average 3%). Two examples of mismatch of VOI_{DWI} and VOI_{PET} can be seen in Fig. 3; a worst case (Fig. 3A) and a representative case (Fig. 3B). It should be noted that due to the relatively small tumor volume in this patient even a small mismatch between T_2 , DWI and PET has a relatively large percent-wise impact in the overlap analysis.

Correlation between SUV and ADC

A scatter plot of SUV_{max} and ADC_{min} can be seen in Fig. 4, both from the first scan (Fig. 4A) and the second scan (Fig. 4B). There were no significant difference in SUV_{max} (mean difference 0.9, $p=0.11$) nor ADC_{min} (mean difference 9.7, $p=0.69$) between the first and the second scan. On a tumor basis, the correlation between SUV_{max} and ADC_{min} was not significant with correlation coefficients of -0.26 ($p = 0.32$) and -0.37 ($p = 0.15$) on scan 1 and 2, respectively. Similarly, no significant difference between SUV_{mean} and ADC_{mean} on scan 1 and 2 was observed ($p=0.9$ and $p=0.5$) and the correlation was not significant (-0.05 ($p = 0.85$) and -0.39 ($p = 0.13$)).

The correlation between ADC and SUV on a voxel-wise level was significantly negative in nine of 12 patients on the first scan. However, the correlation coefficients were small suggesting only a weak correlation (mean correlation coefficient $\rho = -0.23$ (range; [-0.63; 0.31]) including data from all 22 scans).

Cluster analysis

The voxel-by-voxel comparison and the cluster analysis proved feasible and in most of the 11 cases reproducible (assessed visually). All results can be seen in table 3 and in the supplement material (Supplemental Fig. 2).

Cluster 2 (red) encompassed most of the VOI_{PET} (median overlap of 91% and 97% on the first and second scan) and the majority of VOI_{DWI} (median overlap 65% and 52% on the first and second scan). Likewise cluster 1 only encompassed a small part of VOI_{DWI} and VOI_{PET} on both scans (Table 3). In most but not all patients, separation between clusters appeared to be defined by a SUV threshold and hence not dependent on ADC (Supplemental Fig. 2)

In Fig. 5 slices from the PET and the DWI scans from the same two patients as in Fig. 3 as well as the correlation plots from the voxel-by-voxel analysis can be seen. The ‘representative overlap’ case (Figs. 5E-H) has clusters defined primarily by a SUV value around 6. For the ‘poor overlap’ case (Figs. 5A-D), conversely, the clusters are not separated by a single SUV value, but depend on both SUV and ADC in a non-trivial manner.

DISCUSSION

The tumor overlap between VOI_{DWI} and VOI_{PET} was not complete but substantial and reproducible with the majority of VOI_{DWI} encompassed in VOI_{PET} (more than 80%) and the majority of VOI_{PET} encompassed in VOI_{DWI} (more than 60%) on both scans. There was no significant correlation between the quantifiable measures SUV_{max} and ADC_{min} across patients, however on a voxel-by-voxel basis the correlation between ADC and SUV was significant, albeit probably too weak to allow any meaningful assessment of one image metric from the other. The cluster analysis proved feasible and reproducible, identifying a volume encompassing the majority of VOI_{PET} and a smaller part of VOI_{DWI} .

With the integrated PET/MR the tumor is assessed simultaneously and the head and neck coil used limits the movement of the patient during scanning. Hence, it is unlikely that a misalignment between the DWI and PET images is the main reason for discrepancy between the volumes VOI_{PET} and VOI_{DWI} . Other technical reasons for the partial overlap include geometric distortions of the DWI signal close to air cavities such as in the pharynx, which may remain despite the optimized DWI acquisition and FUGUE correction. Both image acquisition and post-processing was optimized to minimize distortions. Visually judged the correspondence of DWI and FDG-PET is overall good as seen in figures(25). After implementation of FUGUE no patient had to be excluded due to signal drop out (Supplemental Fig. 1). The remaining part of the observed mismatch is likely due to a biological difference; i.e. intra-tumor heterogeneity. Thus when minimizing the mismatch due to repositioning and technical distortions, the method presented here might have the potential to identify and describe areas of the tumor with different biological characteristics which is a prerequisite for personalized treatment in the future.

Dose painting is a novel concept in radiotherapy where the radiation dose is escalated in parts of the tumor thought to be treatment resistant such as hypoxic regions or regions with high pre-treatment

FDG uptake(27,28). Tumor areas with high glucose uptake and/or high cellularity are hypothesized as relevant targets for dose painting(17,29) and if the tumor sub-volumes defined by DWI and FDG PET is identical it could in theory be possible to replace FDG with another PET tracer without significant loss of information when imaged simultaneously with DWI on an integrated PET/MR. The replacement of FDG with another PET tracer could provide additional potentially important information of tumor biology. For instance tumor sub-regions with high proliferation (^{18}F -FLT), hypoxia (^{18}F -FAZA) or markers for aggressiveness, e.g. urokinase-type plasminogen activator receptor PET would be interesting not only in terms of multiparametric imaging research but also of potential clinical relevance(30,31). These sub-regions might be used to for treatment guidance such as in dose painting or be used to select patients for other more aggressive treatments regimens in the future. The tumor overlap of VOI_{DWI} and VOI_{PET} assessed in this study is substantial but nevertheless only partial, and together with the relatively weak correlation between image surrogates of high cellularity (assessed with DWI) and high glucose uptake (assessed with FDG PET) our results indicate that the two imaging modalities provide complementary information on tumor biology. Moreover these sub-volumes of the tumor seem to be stable over time both with regard to quantitative ADC and SUV values and spatial placement. The reproducibility of the FDG measurements have been documented in another study(23) but the reproducibility of the ADC values have not previously been assessed.

The partial overlap demonstrated in this study is in concordance with the study by Houweling et al. (32). Thus, substituting one modality with the other is not possible without some loss of information. It can also be concluded that replacing FDG PET with DWI for tumor delineation would yield smaller target volumes in radiotherapy, potentially missing substantial tumor volume as defined by FDG PET. It is also possible that the sub-volume identified by the cluster-analysis based on information from both DWI and FDG PET could be a potential target for dose-escalation. But this needs confirmation in studies with histological correlation or failure pattern analysis(33). It could be argued that the cluster analysis did not seem to provide further useful information than the overlap analysis from the manual delineated tumor volumes (VOI_{PET} and VOI_{DWI}). Nevertheless, the substantial overlap of information from DWI and FDG PET may be encouraging if non-FDG is to be used as part of PET/MR imaging.

To our knowledge, only one study has evaluated the correlation between DWI and FDG PET on an integrated PET/MR scanner in patients with HNSCC(6). This study also reported a negative correlation, however the study only included seven patients with different tumor subsites(6). The existing studies in the literature are either not performed on an integrated PET/MR or not including patients with head and neck tumors (21,22,34–38). The non-significant correlation found across patients suggests that information on glucose metabolism and cellularity from only one voxel, either the voxel within the tumor with the highest FDG-uptake (SUV_{max}) or the lowest diffusion (ADC_{min}), may be too crude to adequately describe the tumor and depict a potential correlation. This is substantiated by the significant correlation reported in most cases in the voxel-by-voxel analysis (Supplemental Fig. 2) nevertheless the weak correlation shows that a biologic mechanistic hypothesis where diffusion of water is uniformly impaired in areas with high glucose metabolism is an oversimplification.

Though the results also in this study seems reproducible from scan 1 to scan 2, the small number of patients is a limitation of this study and there could be true correlations that the sample size is too small to detect. Moreover, the tumors in this patient cohort are relatively small and the application of voxel-by-voxel analysis for description of tumor heterogeneity will probably be more relevant and provide more information in larger tumors.

CONCLUSION

In multiparametric imaging with integrated PET/MR the VOIs from DWI and FDG PET were both within the target volume for radiotherapy and overlapped substantially although not completely. This is important for further research in tumor biology and may have implications for the use of PET/MR for radiotherapy in head and neck cancer and possibly in other malignancies. No significant correlation between FDG uptake and DWI could be found across patients. However, in individual patients a weak correlation could be found on a voxel-by-voxel basis. This suggests that, despite the partial tumor overlap, FDG PET and DWI detects different aspects of tumor biology, and they may possibly have complimentary roles in target definition for dose painting which should be explored further with histological validation.

ACKNOWLEDGEMENTS:

JHR acknowledges support from the Arvid Nilssons Foundation.

REFERENCES

1. Vogelstein B, Papadopoulos N, Velculescu VE, Zhou S, Diaz LA, Kinzler KW. Cancer genome landscapes. *Science*. 2013;339:1546–1558.
2. Gerlinger M, Rowan AJ, Horswell S, et al. Intratumor heterogeneity and branched evolution revealed by multiregion sequencing. *N Engl J Med*. 2012;366:883–892.
3. Yap TA, Gerlinger M, Futreal PA, Pusztai L, Swanton C. Intratumor heterogeneity: seeing the wood for the trees. *Sci Transl Med*. 2012;4:127ps10.
4. O'Connor JPB, Rose CJ, Waterton JC, Carano RAD, Parker GJM, Jackson A. Imaging Intratumor Heterogeneity: Role in Therapy Response, Resistance, and Clinical Outcome. *Clin Cancer Res*. 2014;21:249–257.
5. Even AJG, De Ruyscher D, Van Elmpt W. The promise of multiparametric imaging in oncology: how do we move forward? *Eur J Nucl Med Mol Imaging*. 2016;43:1195–1198.
6. Leibfarth S, Simoncic U, Mönnich D, et al. Analysis of pairwise correlations in multi-parametric PET/MR data for biological tumor characterization and treatment individualization strategies. *Eur J Nucl Med Mol Imaging*. 2016;43:1199–1208.
7. Balyasnikova S, Löfgren J, de Nijs R, Zamogilnaya Y, Højgaard L, Fischer BM. PET/MR in oncology: an introduction with focus on MR and future perspectives for hybrid imaging. *Am J Nucl Med Mol Imaging*. 2012;2:458–474.
8. Buchbender C, Heusner T a, Lauenstein TC, Bockisch A, Antoch G. Oncologic PET/MRI, part 1: tumors of the brain, head and neck, chest, abdomen, and pelvis. *J Nucl Med*. 2012;53:928–938.
9. Platzek I, Beuthien-Baumann B, Schneider M, et al. PET/MRI in head and neck cancer: initial experience. *Eur J Nucl Med Mol Imaging*. 2013;40:6–11.
10. Stransky N, Egloff AM, Tward AD, et al. The mutational landscape of head and neck squamous cell carcinoma. *Science*. 2011;333:1157–1160.

11. Leemans CR, Braakhuis BJM, Brakenhoff RH. The molecular biology of head and neck cancer. *Nat Rev Cancer*. 2011;11:9–22.
12. Lawrence MS, Sougnez C, Lichtenstein L, et al. Comprehensive genomic characterization of head and neck squamous cell carcinomas. *Nature*. 2015;517:576–582.
13. Rasmussen JH, Vogelius IR, Fischer BM, et al. Prognostic value of 18F-Fludeoxyglucose uptake in 287 patients with head and neck squamous cell carcinoma. *Head Neck*. 2015;37:1274-1281
14. Lambrecht M, Van Calster B, Vandecaveye V, et al. Integrating pretreatment diffusion weighted MRI into a multivariable prognostic model for head and neck squamous cell carcinoma. *Radiother Oncol*. 2014;110:429–434.
15. Becker M, Zaidi H. Imaging in head and neck squamous cell carcinoma: the potential role of PET/MRI. *Br J Radiol*. 2015;88(1048):20140655.
16. Kwee TC, Takahara T, Ochiai R, et al. Complementary roles of whole-body diffusion-weighted MRI and 18F-FDG PET: the state of the art and potential applications. *J Nucl Med*. 2010;51:1549–1558.
17. Bentzen SM, Gregoire V. Molecular imaging-based dose painting: a novel paradigm for radiation therapy prescription. *Semin Radiat Oncol*. 2011;21:101–110.
18. Grueneisen J, Beiderwellen K, Heusch P, et al. Correlation of standardized uptake value and apparent diffusion coefficient in integrated whole-body PET/MRI of primary and recurrent cervical cancer. *PLoS One*. 2014; 9(5): e96751.
19. Heusch P, Buchbender C, Köhler J, et al. Correlation of the apparent diffusion coefficient (ADC) with the standardized uptake value (SUV) in hybrid 18F-FDG PET/MRI in non-small cell lung cancer (NSCLC) lesions: initial results. *RöFo*. 2013 Nov;185(11):1056-62.
20. Ho K-C, Lin G, Wang J-J, Lai C-H, Chang C-J, Yen T-C. Correlation of apparent diffusion coefficients measured by 3T diffusion-weighted MRI and SUV from FDG PET/CT in primary cervical cancer. *Eur J Nucl Med Mol Imaging*. 2009;36:200–208.

21. Schmidt H, Brendle C, Schraml C, et al. Correlation of simultaneously acquired diffusion-weighted imaging and 2-deoxy-[18F] fluoro-2-D-glucose positron emission tomography of pulmonary lesions in a dedicated whole-body magnetic resonance/positron emission tomography system. *Invest Radiol*. 2013;48:247–255.
22. Metz S, Ganter C, Lorenzen S, et al. Multiparametric MR and PET Imaging of Intratumoral Biological Heterogeneity in Patients with Metastatic Lung Cancer Using Voxel-by-Voxel Analysis. *PLoS One*. 2015;10:e0132386
23. Rasmussen JH, Fischer BM, Aznar MC, et al. Reproducibility of FDG PET uptake measurements in head and neck squamous cell carcinoma on both PET/CT and PET/MR. *Br J Radiol*. 2015;88:20140655.
24. Delso G, Furst S, Jakoby B, et al. Performance Measurements of the Siemens mMR Integrated Whole-Body PET/MR Scanner. *J Nucl Med*. 2011;52:1914–1922.
25. Hansen AE, Rasmussen J, Johannesen HH, et al. Geometric distortions of diffusion weighted imaging of the head/neck in combined PET/MR: optimization of image acquisition and post-processing correction for oncology applications. *EJNMMI Phys*. 2014;1:A76.
26. Bayne M, Hicks RJ, Everitt S, et al. Reproducibility of “intelligent” contouring of gross tumor volume in non-small-cell lung cancer on PET/CT images using a standardized visual method. *Int J Radiat Oncol Biol Phys*. 2010;77:1151–1157.
27. Bentzen SM. Theragnostic imaging for radiation oncology: dose-painting by numbers. *Lancet Oncol*. 2005;6:112–117.
28. Tanderup K, Olsen DR, Grau C. Dose painting: art or science? *Radiother Oncol*. 2006;79:245–248.
29. Dirix P, Vandecaveye V, De Keyser F, Stroobants S, Hermans R, Nuyts S. Dose painting in radiotherapy for head and neck squamous cell carcinoma: value of repeated functional imaging with (18)F-FDG PET, (18)F-fluoromisonidazole PET, diffusion-weighted MRI, and dynamic contrast-enhanced MRI. *J Nucl Med*. 2009;50:1020–1027.

30. Bailey DL, Antoch G, Bartenstein P, et al. Combined PET/MR: The Real Work Has Just Started. Summary Report of the Third International Workshop on PET/MR Imaging. *Mol Imaging Biol.* 2015; 25672749.
31. Persson M, Skovgaard D, Brandt-Larsen M, et al. First-in-human uPAR PET: Imaging of Cancer Aggressiveness. *Theranostics.* 2015;5:1303–1316.
32. Houweling AC, Wolf AL, Vogel W V, et al. FDG-PET and diffusion-weighted MRI in head-and-neck cancer patients: implications for dose painting. *Radiother Oncol.* 2013;106:250–254.
33. Due AK, Vogelius IR, Aznar MC, et al. Recurrences after intensity modulated radiotherapy for head and neck squamous cell carcinoma more likely to originate from regions with high baseline [18F]-FDG uptake. *Radiother Oncol.* 2014;111:360–365.
34. Choi SH, Paeng JC, Sohn C-H, et al. Correlation of 18F-FDG uptake with apparent diffusion coefficient ratio measured on standard and high b value diffusion MRI in head and neck cancer. *J Nucl Med.* 2011;52:1056–1062.
35. Fruehwald-Pallamar J, Czerny C, Mayerhoefer ME, et al. Functional imaging in head and neck squamous cell carcinoma: correlation of PET/CT and diffusion-weighted imaging at 3 Tesla. *Eur J Nucl Med Mol Imaging.* 2011;38:1009–1019.
36. Nakajo M, Kajiya Y, Kaneko T, et al. FDG PET/CT and diffusion-weighted imaging for breast cancer: prognostic value of maximum standardized uptake values and apparent diffusion coefficient values of the primary lesion. *Eur J Nucl Med Mol Imaging.* 2010;37:2011–2020.
37. Nakamatsu S, Matsusue E, Miyoshi H, Kakite S, Kaminou T, Ogawa T. Correlation of apparent diffusion coefficients measured by diffusion-weighted MR imaging and standardized uptake values from FDG PET/CT in metastatic neck lymph nodes of head and neck squamous cell carcinomas. *Clin Imaging.* 2012;36:90–97.
38. Varoquaux A, Rager O, Lovblad K-O, et al. Functional imaging of head and neck squamous cell carcinoma with diffusion-weighted MRI and FDG PET/CT: quantitative analysis of ADC and SUV. *Eur J Nucl Med Mol Imaging.* 2013;40:842–852.

Tables:

	...1. scan	No. of patients from 2. Scan
PET data	17	17
ADC data	17	17
Data for voxel by voxel analysis	12	12

Table 1. Patients with data available for voxel-wise comparison from the first respectively second scan with regard to PET, ADC and post processing (FUGUE) which is necessary to perform voxel by voxel comparison.

	Scan 1 Median (range)	Scan 2 Median (range)
VOI_{PET} (cc)	8.0 (1.2-25.2)	8.3 (1.6-24.8)
VOI_{DWI} (cc)	5.6 (0.7-17.8)	5.8 (1.1-17.0)
GTV_{T2} (cc)	16.1 (5.8-36.2)	16.5 (7.8-36.7)
VOI_{PET} in VOI_{DWI} (%)	61.5 (40.0-86.0)	59.5 (42.0-79.0)
VOI_{DWI} in VOI_{PET} (%)	81.5 (58.0-94.0)	84.5 (48.0-100)
VOI_{DWI} in GTV_{T2} (%)	97.0 (82.0-100)	98.0 (84.0-100)
VOI_{PET} in GTV_{T2} (%)	97.5 (90.0-100)	99.5 (89.0-100)

Table 2. Median tumor volume from DWI, FDG PET and anatomical T₂ weighted MR in cc. The tumor overlap between each modality is reported in percent.

	Scan 1 Median (range)	Scan 2 Median (range)
Cluster1 in VOI_{DWI} (%)	14.4 (0.1-32.1)	12.6 (0.4-24.6)
Cluster1 in VOI_{PET} (%)	14.6 (2.6-45.6)	13.8 (0-60.2)
Cluster2 in VOI_{DWI} (%)	65.4 (33.7-82.1)	51.8 (28.8-88.6)
Cluster2 in VOI_{PET} (%)	90.5 (59.4-97.9)	97.2 (55.7-97.9)

Table 3. The overlap between the two clusters and GTV defined from DWI and FDG PET/MR is reported in percent.

Figures and legends

Figure 1

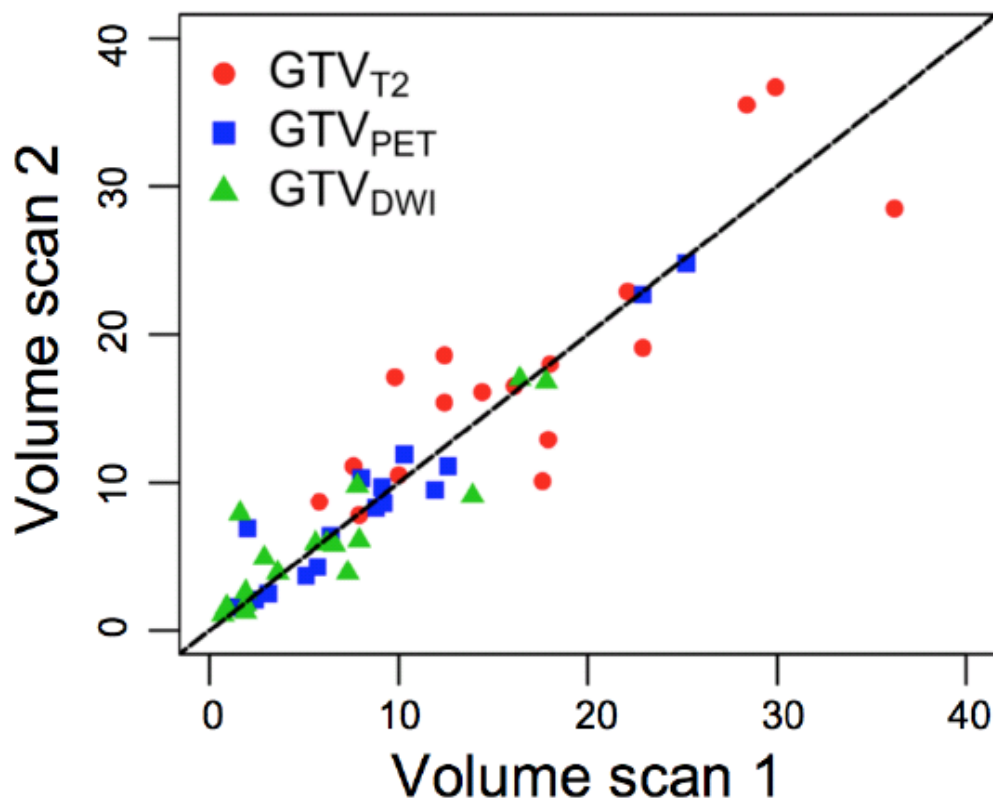


Figure 1. Tumor volumes measured with diffusion weighted imaging (VOI_{DWI}), PET imaging (VOI_{PET}) and with anatomical T_2 imaging (GTV_{T_2}) on the two PET/MR scans.

Figure 2.

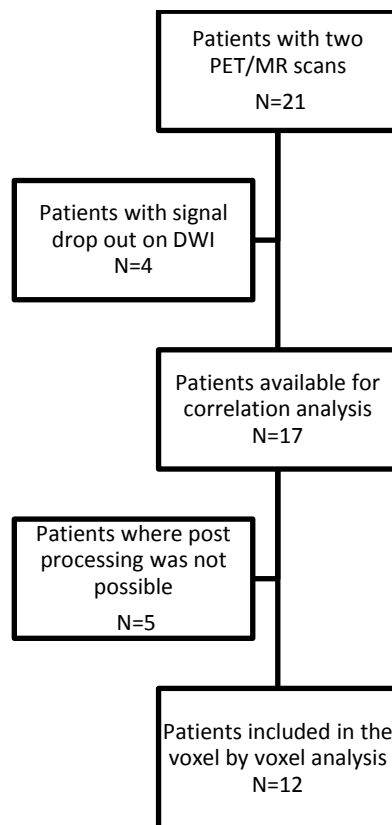


Figure 2. Flowchart of patients included.

Figure 3

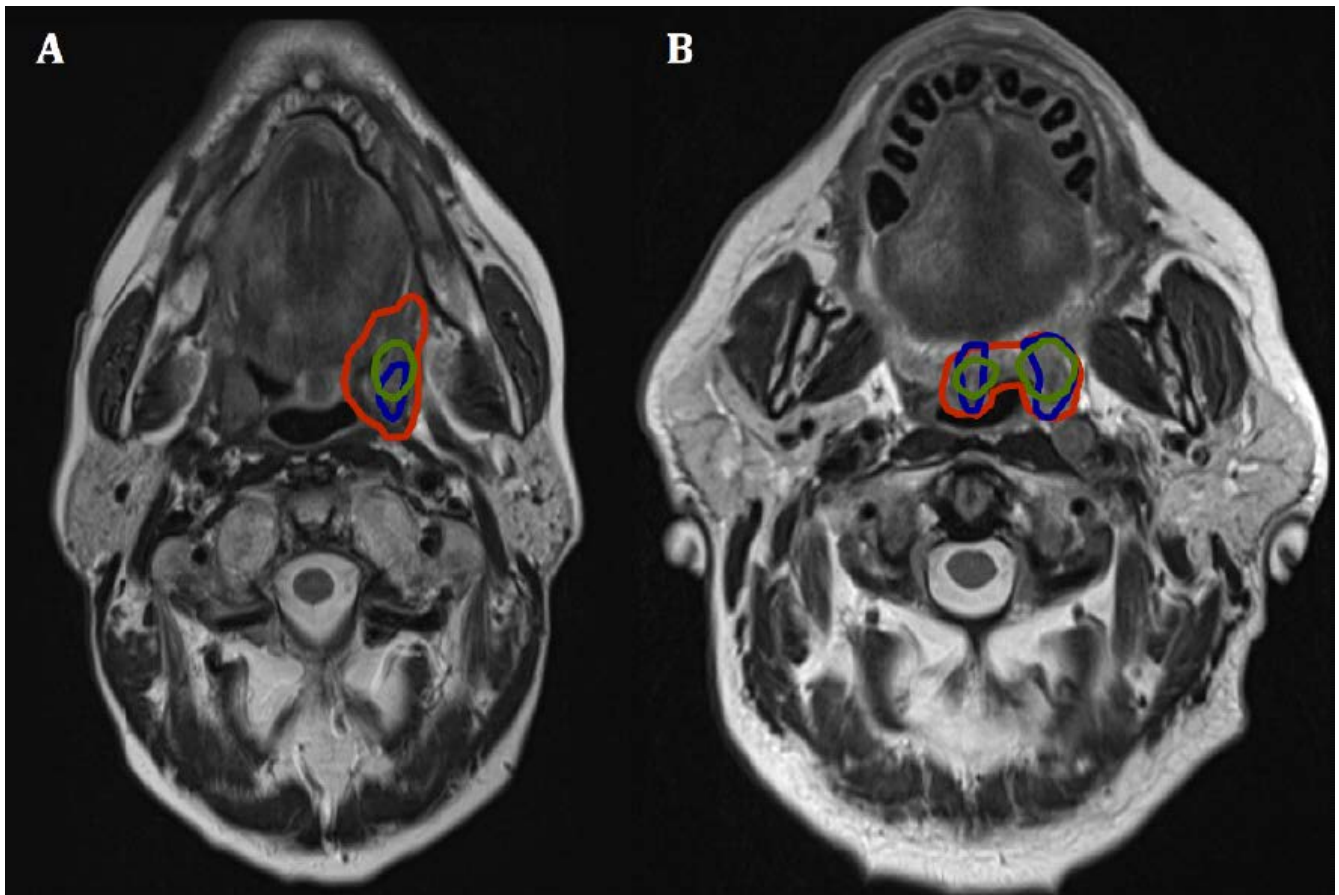


Figure 3. Examples of tumor overlap between tumor defined from diffusion weighted imaging (blue contour), tumor defined from FDG PET/MR (green contour) and T2 weighted MR (red contour). Fig. 3A illustrates the worst case of overlap between VOI_{DWI} and VOI_{PET} . Forty-two percent of VOI_{PET} is within the VOI_{DWI} and 63% of VOI_{DWI} is within the VOI_{PET} . Fig. 3B illustrates a representative case where 67% of VOI_{PET} is within the VOI_{DWI} and 68% of VOI_{DWI} is within the VOI_{PET} .

Figure 4

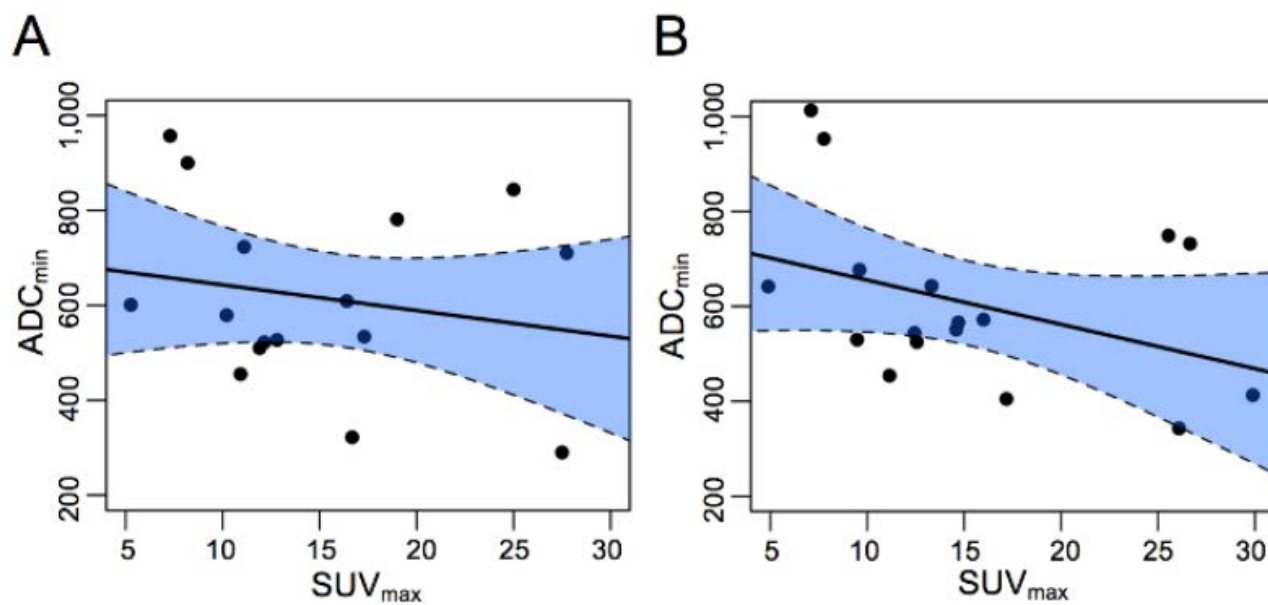


Figure 4. Scatterplot of SUV_{max} and ADC_{min} from the first scan (A) and from the second scan (B). The data is fitted to a linear model, and layed over with a 95% confidence-interval (blue).

Figure 5

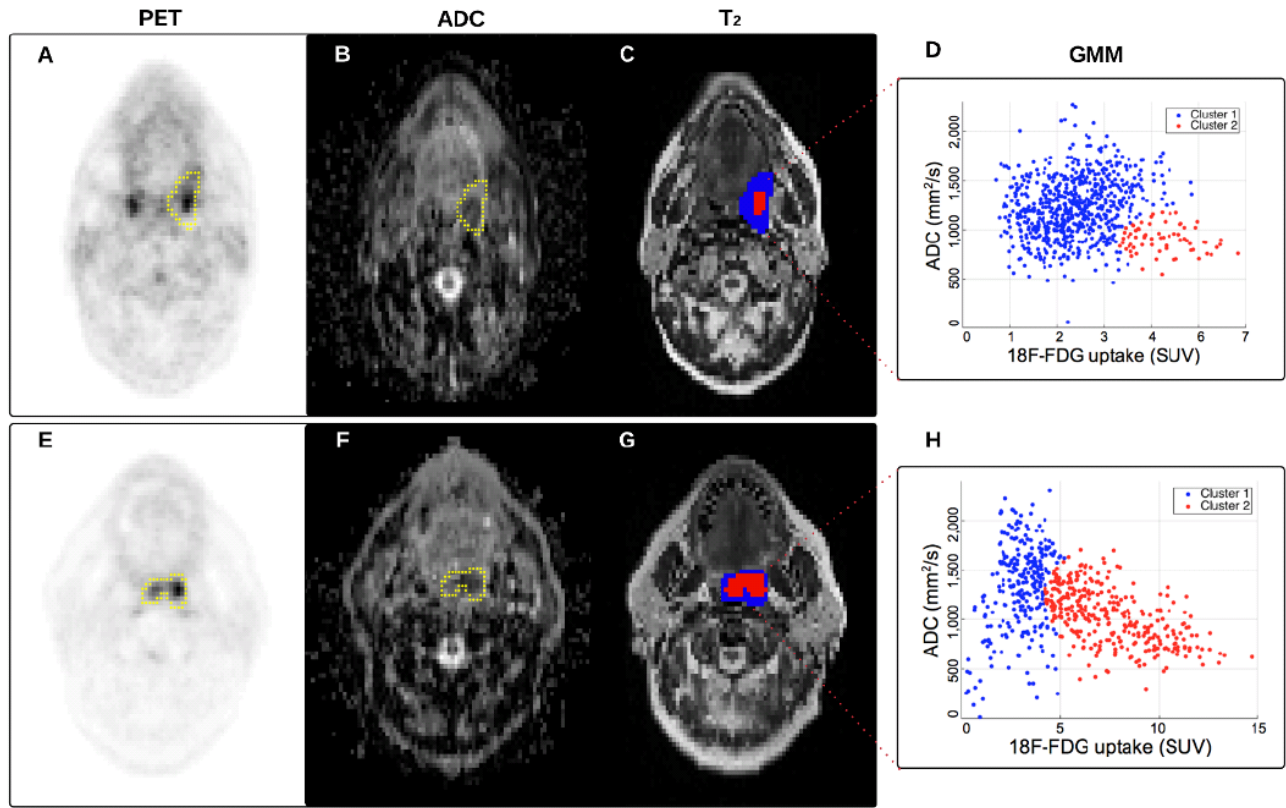
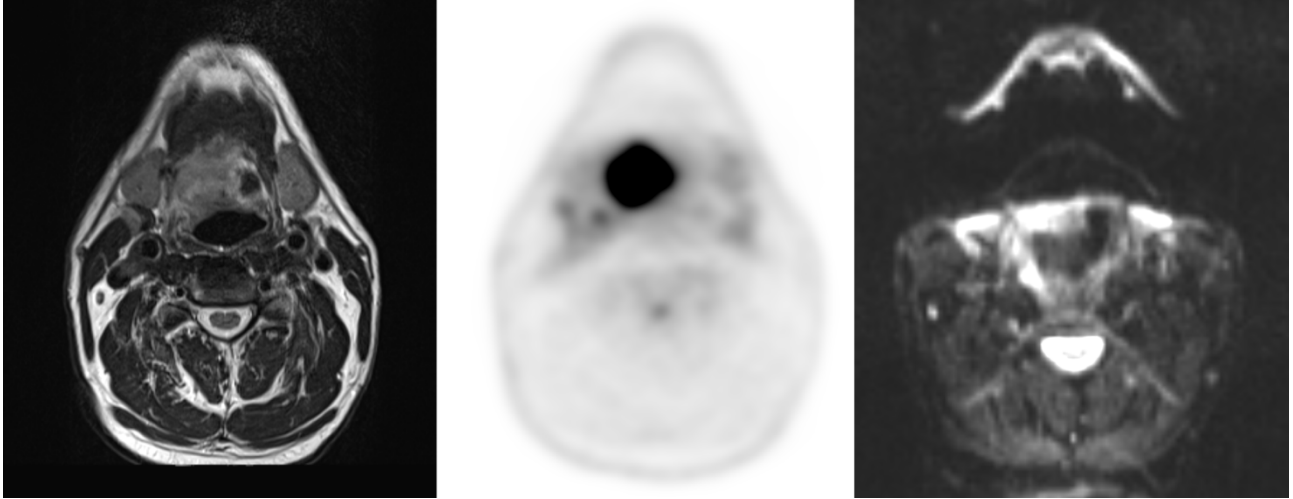


Figure 5. PET image (A) image from the ADC map (B) and T₂-weighted image (C) from the patient in Fig. 3A (“poor overlap” case). The yellow contour represents GTV_{T₂}. (D) is the scatter plot from the voxel-by-voxel analysis showing the respective clustering assignment from the cluster analysis. (E), (F) and (G) show the PET image, ADC map and T₂ image for the patient in Fig. 3B (“representative overlap” case) and H shows the scatter plot and the clustering assignment from the cluster analysis.

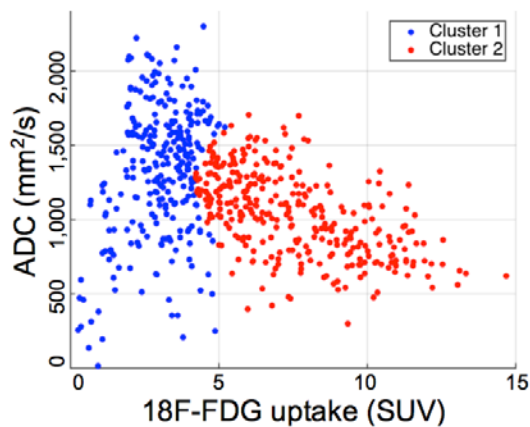
Supplement material

Supplemental Figure 1. Example from a case with a large signal drop out on the DWI (right panel). In the left panel is the T2 weighted image and in the middle panel the PET image.

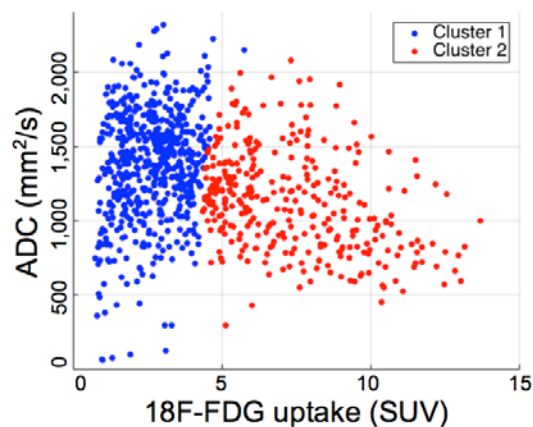


Supplemental Figure 2. Cluster analysis of the correlation plot for the 11 patients included in the voxel by voxel analysis, numbered after study number. Panel to the left is from the first scan, panel to right is from the second scan. ρ is Spearman's rank correlation coefficient.

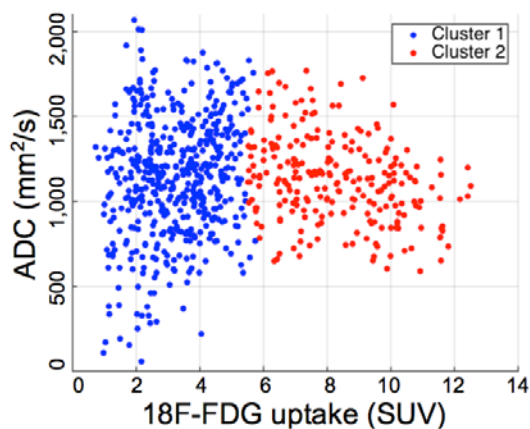
$\rho = -0.41$ ($P < 0.0001$)



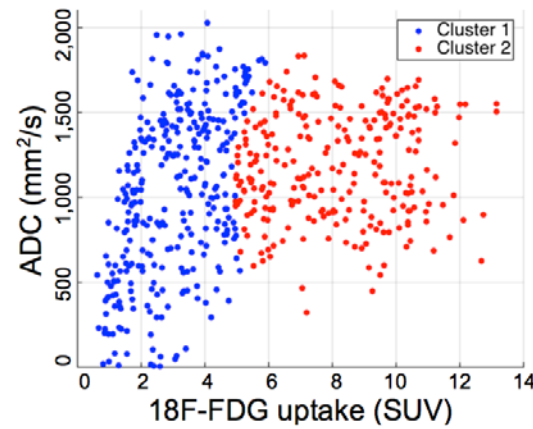
$\rho = -0.26$ ($P < 0.0001$)



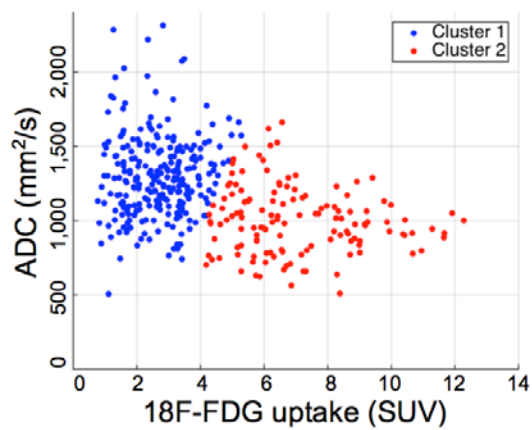
$\rho = 0.006$ ($P = 0.86$)



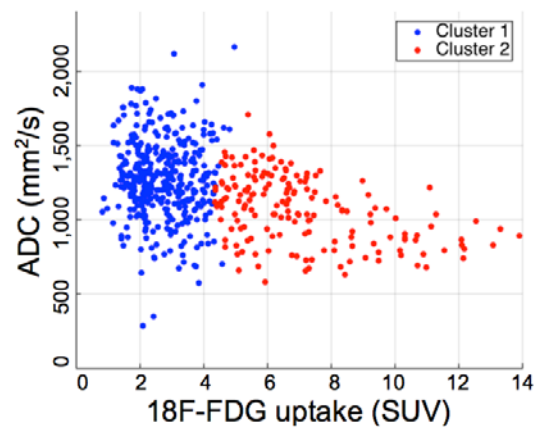
$\rho = 0.31$ ($P < 0.0001$)



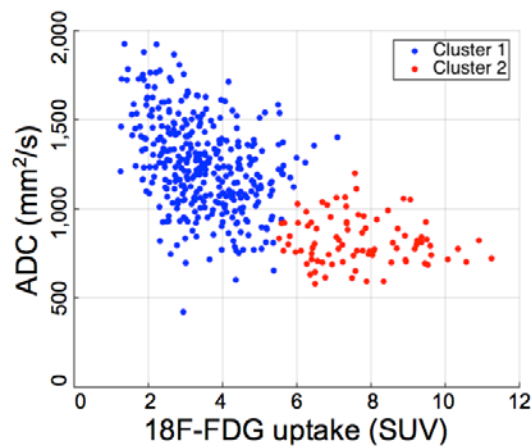
$\rho = -0.39$ ($P < 0.0001$)



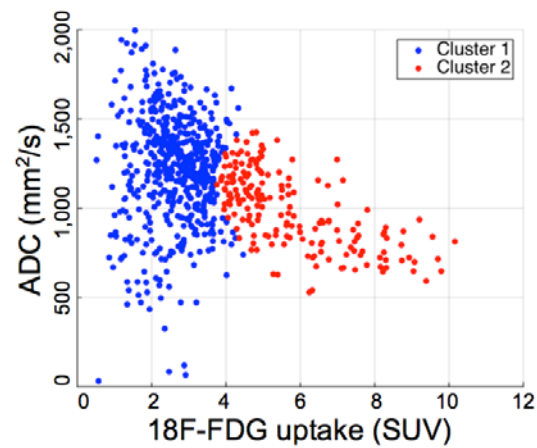
$\rho = -0.36$ ($P < 0.0001$)



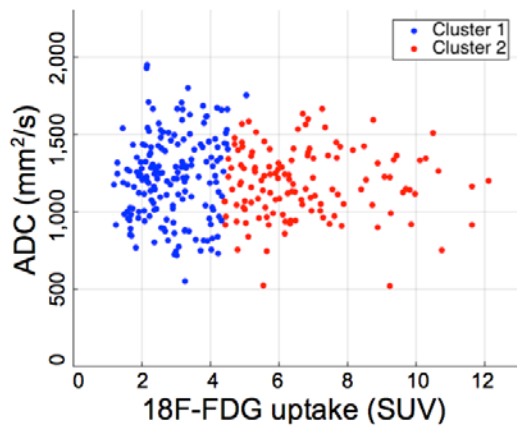
$\rho = -0.62$ ($P < 0.0001$)



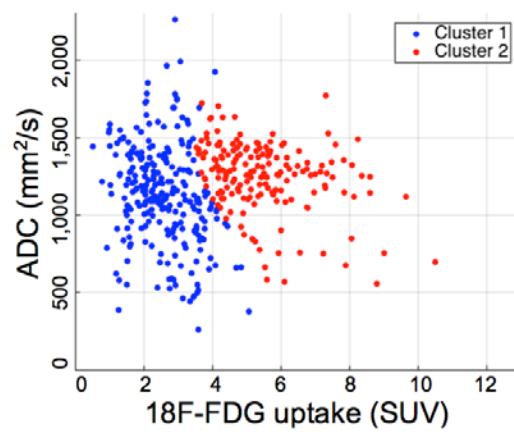
$\rho = -0.36$ ($P < 0.0001$)



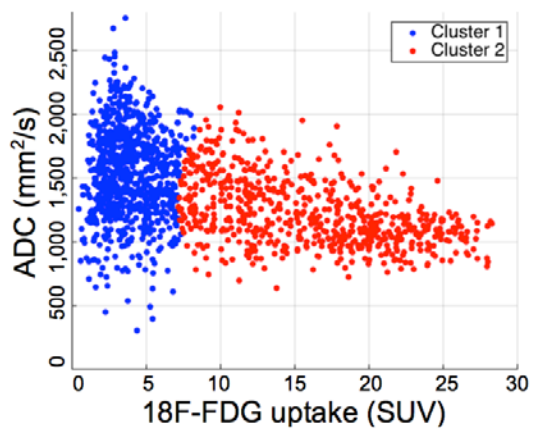
$\rho = -0.001$ ($P = 0.93$)



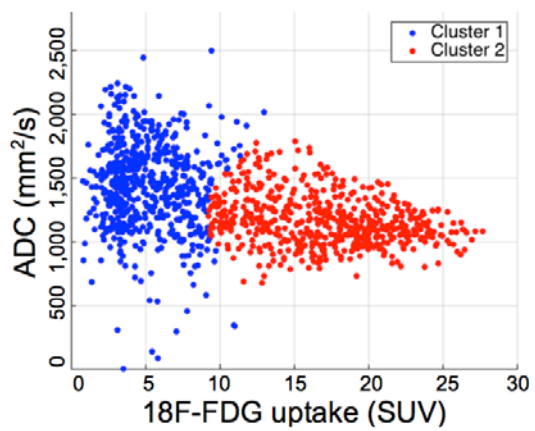
$\rho = 0.03$ ($P = 0.57$)



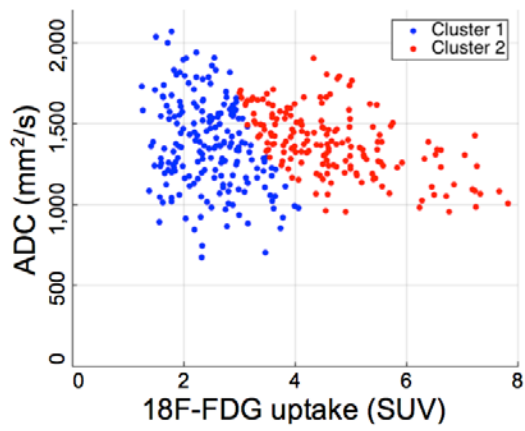
$\rho = -0.47$ ($P < 0.0001$)



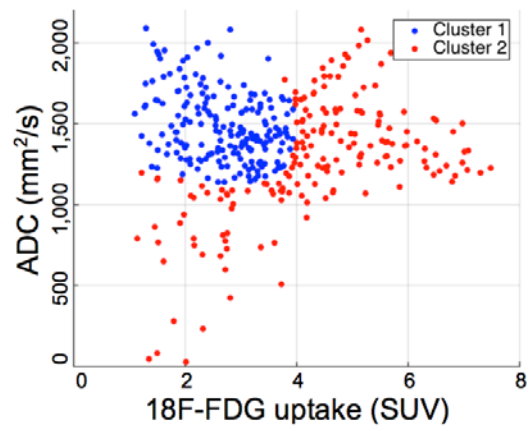
$\rho = -0.48$ ($P < 0.0001$)



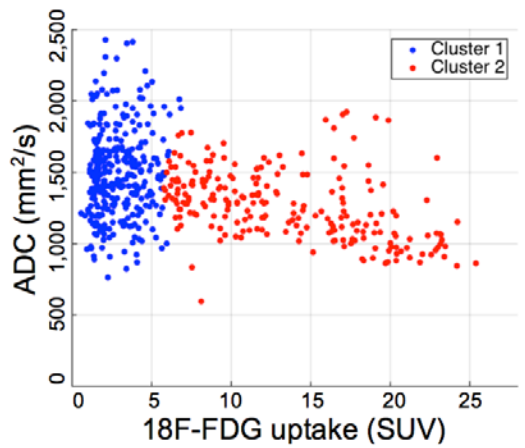
$\rho = -0.18$ ($P = 0.0006$)



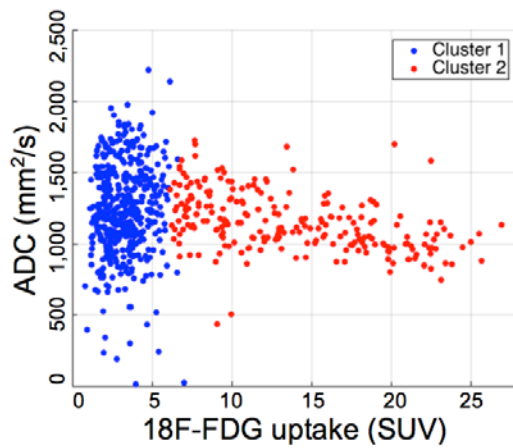
$\rho = 0.00$ ($P = 0.998$)



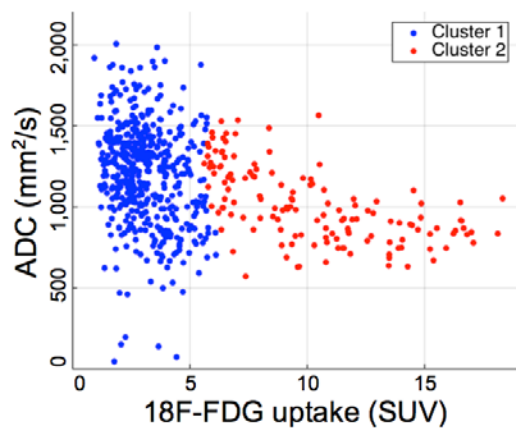
$\rho = -0.36$ ($P < 0.0001$)



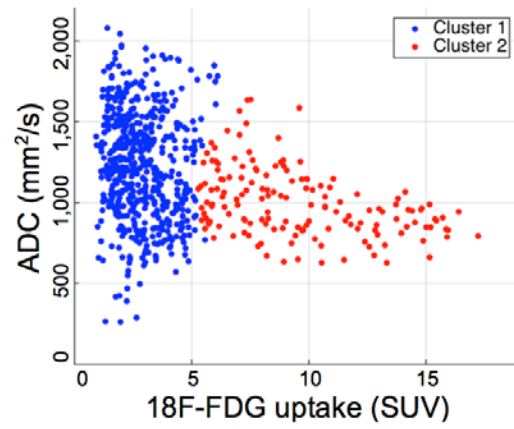
$\rho = -0.16$ ($P < 0.0001$)



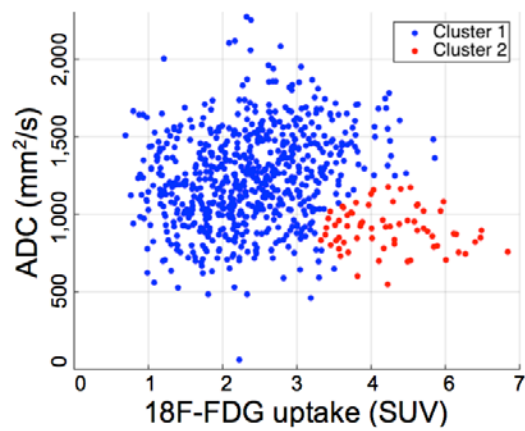
$\rho = -0.38$ ($P < 0.0001$)



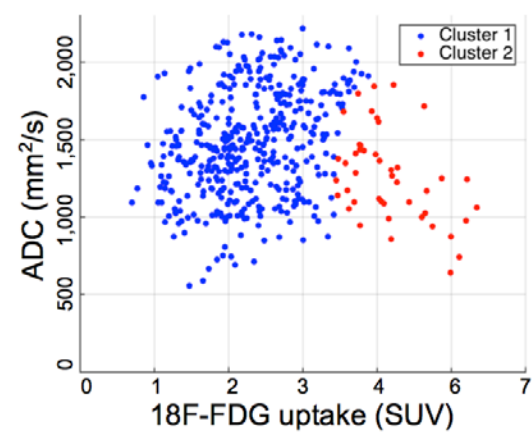
$\rho = -0.32$ ($P < 0.0001$)



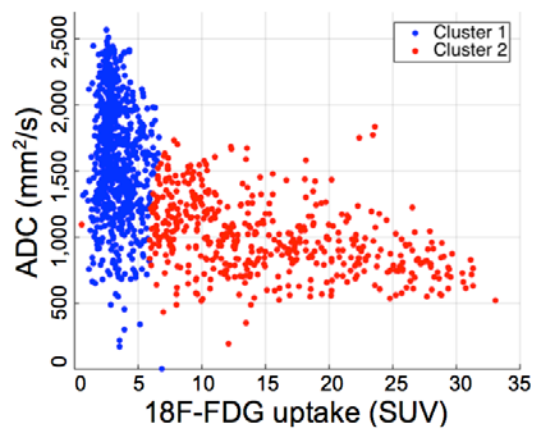
$\rho = 0.05$ ($P = 0.19$)



$\rho = 0.14$ ($P = 0.003$)



$\rho = -0.61$ ($P < 0.0001$)



$\rho = -0.28$ ($P < 0.0001$)

